Pergamon

Geochimica et Cosmochimica Acta, Vol. 68, No. 8, pp. 1827–1835, 2004

0016-7037/04 $30.00 + .00

doi:10.1016/j.gca.2003.10.020

Equation of state of water based on speeds of sound measured in the diamond-anvil cell

EVAN H. ABRAMSON* and J. MICHAEL BROWN
Department of Earth and Space Sciences, University of Washington, Seattle, WA 98195, USA

(*Received April* 18, 2003; *accepted in revised form October* 23, 2003)

Abstract—Measurements of the speed of sound in water have been extended to 5.5 GPa and 400°C. The data were taken in the diamond-anvil cell using Impulsive Stimulated Scattering (Forced Rayleigh Scattering) at acoustic frequencies of ~1 GHz. Measured sound speeds differ significantly from those given by previously published equations of state; at 5 GPa, measured speeds are 3% lower than those predicted by the 1995 formulation of the International Association for the Properties of Water and Steam (IAPWS). New thermal diffusivity measurements to 1 GPa are combined with previously reported thermal conductivities in a determination of specific heat. A complete equation of state (giving all thermodynamic quantities) was generated and subsequently extended to 40 GPa and 3000 K. This equation of state matches both our speed of sound data and previously published shock wave data; in a range extending to 3 GPa and 700–1600°C predicted densities are up to 5% higher than those reported from studies of inclusions, leading to a reinterpretation of those previous studies. Within the range of the new data, an experimentally determined estimate of uncertainty is given for the densities.

1. INTRODUCTION

A knowledge of the thermodynamic equation of state (EOS) of fluid water is necessary to our understanding of many phenomena within the purview of the earth and planetary sciences. Pressures and temperatures of interest exceed 12 GPa and 1200 K. Unfortunately, data are sparse at pressures beyond a few tenths of GPa; over 1 GPa, data are available only from shock studies (Walsh and Rice, 1957; Kormer, 1968; Lyzenga et al., 1982; Mitchell and Nellis, 1982), previous measurements of speed of sound to 3.5 GPa and 200°C (Wiryana et al., 1998), volume measurements deriving both from inclusion studies (Brodholt and Wood, 1994; Frost and Wood, 1997; Withers et al., 2000) and also the irreversible distension of a platinum vessel (Larrieu and Ayers, 1997), and the early (differential) volume measurements of Bridgman (1942). Equations of state for water, at high pressures, rely heavily on extrapolation of data, calculations of molecular dynamics, or a combination of both (Haar et al., 1984; Saul and Wagner, 1989; Belonoshko and Saxena, 1991; Holland and Powell, 1991; Brodholt and Wood, 1993; Pitzer and Sterner, 1994; Wagner and Pruss, 2002); several of these are in common use although their differences are significant (see, e.g., Brodholt and Wood, 1993). Clearly, further experimental data are required to accurately extend water's EOS to pressures exceeding 1 GPa.

We previously reported speeds of sound to 3.5 GPa and 200°C. Here we report a significant extension of this work to 5.5 GPa and 400°C, along with several determinations of specific heat to 0.8 GPa. These expanded data allow us to determine the integrated increase of density with pressure and thus to develop an EOS in this new regime of pressure and temperature; an experimentally supported estimate of uncertainty is given. Comparison of the new results with published shock data leads to a credible extension of the EOS up to 40 GPa and 3000 K.

* Author to whom correspondence should be addressed (evan@ess.washington.edu).

2. EXPERIMENTAL

2.1. Speeds of Sound

A diamond-anvil cell, located within a vacuum furnace, holds water at the desired pressure and temperature. Three chromel-alumel thermocouples affixed to the cell are used to determine temperature to within 1°C. Optical access is obtained through the backs of the diamonds. An 80 ps pulse from a Q-switched, mode-locked, Nd:YAG laser is first split into two and then recombined within the sample at an included angle of 2θ. Interference establishes a spatially periodic distribution of intensity with period $d = \lambda/2\sin\Theta$, where λ, the laser wavelength, is 1064 nm and for these experiments $d \approx 3\ \mu$m. Thermal pressure caused by absorption of the light then impulsively launches counter-propagating, acoustic waves of wavelength d. These waves induce a temporally and spatially periodic variation of index of refraction from which a probe laser (532 nm) can be coherently scattered. The intensity of the scattered probe, modulated at the acoustic frequency, constitutes the signal. The acoustic wavelength, d, varies slowly (and minutely) over hours as a result of slight changes in the positions of optical components (due to thermal expansion or mechanical drift of mounts) and is most easily measured as the ratio of the known speed of sound of a standard substance (normally a previously calibrated piece of glass) to the acoustic frequency generated in that standard. The speed of sound in the sample is then given by the product of its measured acoustic frequency and d. In these experiments, speed of sound is typically determined with a precision of 0.2% (Abramson et al., 1999b; Wiryana et al., 1998). Systematic velocity errors associated with the calibration of the glass standard against water at 1 bar are estimated to be no larger than 0.1%.

2.2. Thermal Diffusivity

After several tens of nanoseconds the acoustic disturbance has disappeared, leaving behind an effectively one-dimensional thermal grating. The diffracted signal from this grating decays with exponential time constant τ which gives the thermal diffusivity, D_{th}, through the equation $\tau = d^2/(8\pi^2 D_{th})$. To achieve the longer (~microsecond) delay times, a second, pulsed laser is used for the probe. Diffusivities are typically measured to 2% (Abramson et al., 1999a; Abramson et al., 2001).

2.3. Pressure Measurement

2.3.1. Ruby

Between 20 and 200°C, pressure was determined by comparison of the fluorescence wavelength of a piece of ruby (Mao et al., 1986)

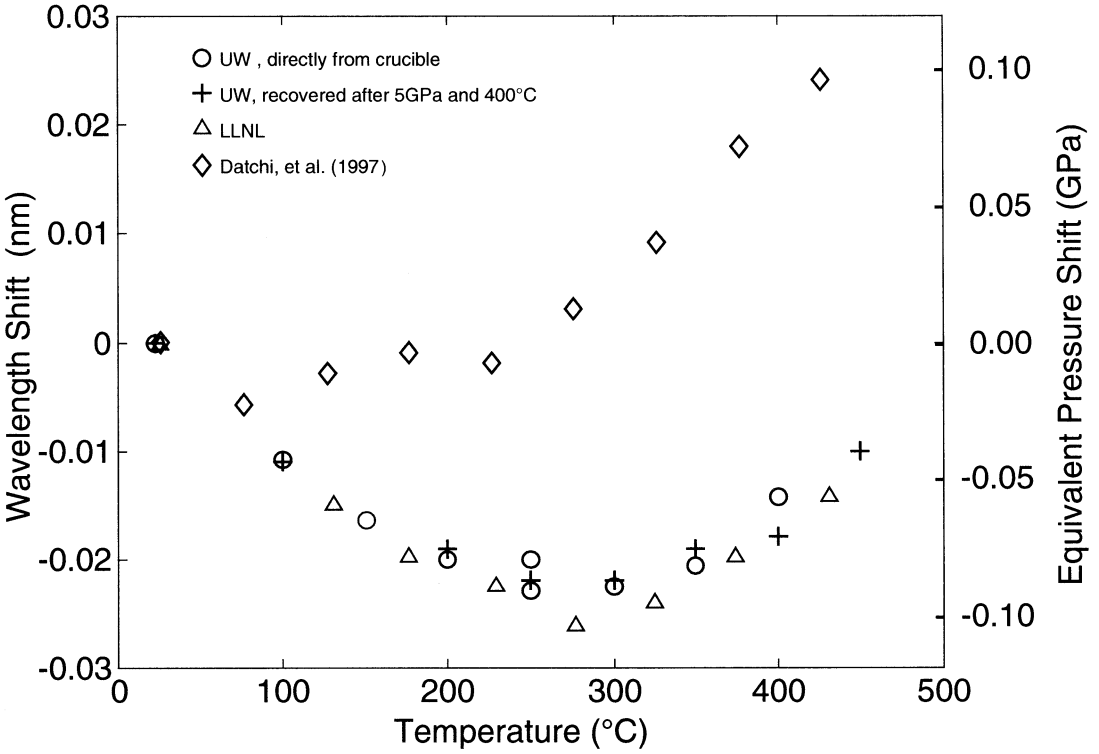

Fig. 1. The temperature-induced shift of the 685.4-nm line of the Sm: SrB_4O_7 pressure standard. The shift in wavelength (left axis) from the value at 25°C is plotted against temperature for a sample taken directly from the crucible (o), another recovered after use to 5 GPa and 400°C (+), a sample obtained from LLNL (Δ), and data reported by Datchi et al. (1997) (◇). Shown on the axis to the right is the amount to be subtracted from the calculated pressure to compensate for the difference in temperature between the reference borate (at 25°C) and the borate in the cell. Differences between this calibration and that of Datchi et al. (1997) are equivalent to as much as 0.13 GPa at 400°C.

within the diamond-anvil cell with that of a second ruby positioned outside the cell (in vacuum) but held at the same temperature. At the lower temperatures, measurements were typically made with a precision of 0.02 GPa, whereas at 200°C precision is degraded to 0.04 GPa due to line-broadening of the fluorescence spectrum.

2.3.2. *Sm:SrB_4O_7*

Above 200°C line broadening renders the ruby pressure gauge insufficiently precise; instead an isolated fluorescence line (685.4 nm) of samarium-doped strontium borate (SrB_4O_7) was used. The fluorescence wavelength of a piece of borate within the diamond-anvil cell was compared with that of a piece at 1 bar and room temperature.

The borate was synthesized in our laboratory as described by Pei et al. (1993) with the addition of 5 mol% samarium and was calibrated against ruby up to 8 GPa and at room temperature in a 16:3:1 by volume solution of methanol, ethanol, and water; this solution is known (Fujishiro et al., 1982) to be a hydrostatic pressure medium under these conditions. Our calibration differs slightly from that previously reported (Datchi et al., 1997, also with respect to ruby), with pressures systematically lower by 0.5 ± 0.1% for a given shift in wavelength (but still within the uncertainty of ~1% claimed by those authors). A calibration of the temperature dependence of the wavelength, however, gave results which differ significantly from the previous report. In Figure 1 the temperature dependence as reported by Datchi et al. (1997) is compared with that of our newly synthesized borate, the same borate recovered after exposure to water at our highest experimental pressures and temperatures, and borate synthesized at Lawrence Livermore National Laboratories. All samples measured in our laboratory are seen to exhibit identical behavior as a function of temperature. The pressure-difference scale on the right side of the figure gives the correction to the calculated pressure necessitated by the temperature dependence; between 200°C and 350°C the correction is largest, reaching 0.09 GPa. Pressures reported here were computed using our calibrations of both pressure-induced and temperature-induced shifts; the sound speed data so recorded demonstrate good continuity between the ruby and borate pressure gauges (see Fig. 4). Within the current range of pressures and temperatures, any cross derivative of the fluorescence wavelength with temperature and pressure is not apparent; we assume that the pressure-induced shift is independent of temperature.

As the borate partially dissolves in water, we followed the lead of Datchi et al. (2000) and divided the load into two volumes, separated by a thin barrier of gold, each of which contains water, but only one of which contains the (partially dissolved) pressure gauge. We found that at room temperature these barriers, with cross-sections of 300 μm × 100 μm and thicknesses of 75 μm, can occasionally support pressure differences of ~0.2 GPa; however, this is unusual and repeated measurements demonstrate a precision of 0.02 GPa with the borate at all temperatures.

3. RESULTS

3.1. Speeds of Sound

Data taken along isotherms of 25, 110, 200, 300, and 400°C are given in Table 1 and plotted as functions of pressure in Figure 2; the three highest pressure points at 25°C are in a fluid metastable with respect to ice VI (Wagner et al., 1994). In the same figure we also show 400°C isotherms predicted by the empirically derived EOS of Wagner and Pruss (2002), and two other EOS derived though molecular dynamics calculations (Belonoshko and Saxena, 1991; Brodholt and Wood, 1993).

Table 1. Measured speeds of sound.

T (°C)	P (GPa)	c (km s^{-1})	T (°C)	P (GPa)	c (km s^{-1})	T (°C)	P (GPa)	c (km s^{-1})
115	1.65	3.182*	22	0.69	2.427	300	5.22	4.424
115	2.19	3.465*	26	1.07	2.765	300	5.56	4.517
115	1.00	2.734*	26	1.39	3.010	400	1.12	2.660
115	1.44	3.065*	200	0.50	2.254	400	1.13	2.660
115	2.29	3.516*	200	1.09	2.800	400	1.14	2.643
100	0.86	2.612*	200	2.77	3.706	400	1.42	2.844
100	1.60	3.161*	200	3.07	3.823	400	2.18	3.304
100	2.15	3.471*	200	3.60	4.020	400	2.61	3.500
100	1.10	2.788*	200	1.14	2.785	400	3.52	3.857
100	1.41	3.028*	200	1.14	2.791	400	3.68	3.923
200	0.94	2.685*	300	1.62	3.059	400	4.70	4.234
200	3.24	3.885*	300	2.20	3.372	400	4.91	4.310
			300	3.62	3.951	400	4.92	4.310
22	1.28	2.931	300	4.53	4.246			

* Previously unpublished data from the study of Wiryana et al. (1998).

None of these curves matches the experimental pressure dependence within the uncertainties, however, the Wagner and Pruss EOS is in accord with the data at the lowest pressures; this observation is developed further below.

3.2. Thermal Diffusivities and Specific Heats

To develop an EOS from the measured speeds of sound, it is necessary to know specific heats as a function of temperature at one, preferably high, pressure. Previous, direct measurements were made to 1 GPa at ~26°C (Czarnota, 1984). However, the lack of an appropriate calibrant led the author to warn of possible pressure-dependent systematic errors. Clearly, it was desirable to obtain more data in this range of pressure.

Specific heat can be calculated as $C_p = K_{th}/(D_{th}\rho)$ where K_{th} is the thermal conductivity, D_{th} the thermal diffusivity, and ρ the density. Measurements of the thermal conductivity of water up to 0.8 GPa and 130°C were reported by Lawson et al. (1959). We (Abramson et al., 2001) previously reported thermal diffusivities of water, and have now added two lower pressure points at 110°C. Together, these data and the known densities can be used to derive the specific heats shown in Figure 3. The uncertainty in C_p based on combining the two data sets is ~3%. Up to 0.9 GPa and 110°C our calculated specific heats are all within 3% of the data of Czarnota (1984) and within 2% of the predictions of the EOS of Wagner and Pruss (2002). This gives confidence in specific heat values used below in the construction of an equation of state.

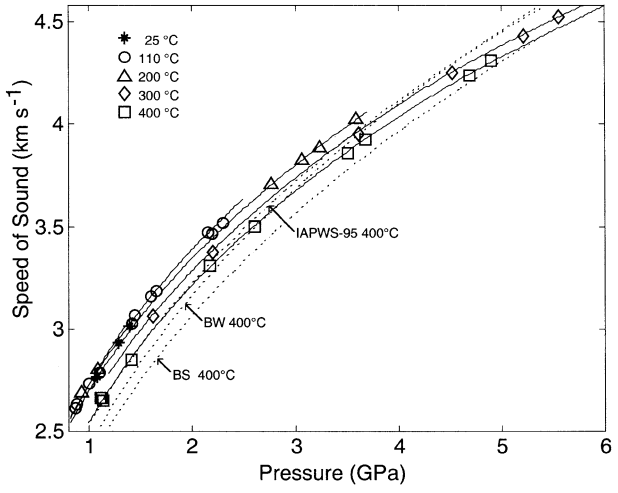

Fig. 2. The measured speeds of sound in water along several isotherms. Continuous lines through the data are calculated using our proposed equation of state. Dashed lines represent 400°C isotherms calculated from IAPWS-95 (Wagner and Pruss, 2002), the equation of state of Brodholt and Wood (1993, BW) and that of Belonoshko and Saxena (1991, BS).

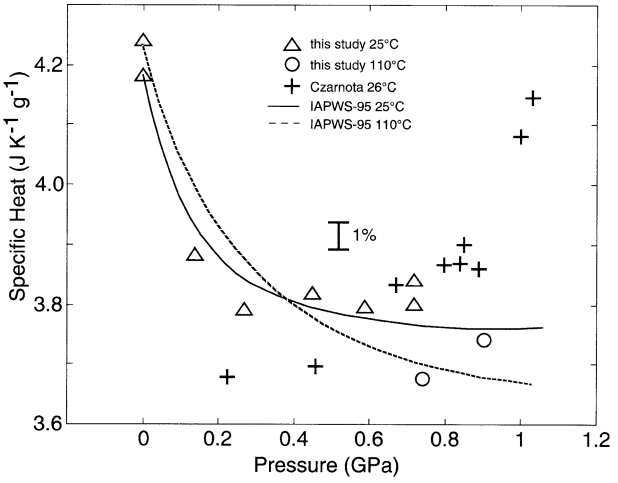

Fig. 3. Specific heats calculated from a combination of our measured thermal diffusivities and the thermal conductivities of Lawson et al. (1959) are plotted against pressure along isotherms of 25°C and 110°C. Also plotted are the data of Czarnota (1984) and results of IAPWS-95 (Wagner and Pruss, 2002).

3.3. Reduction to an Equation of State

3.3.1. Method

Measured speeds of sound are inverted to give an EOS by recursive solution of the combined equations:

$$\left(\frac{\delta\rho}{\delta\rho}\right)_T = \frac{1}{c^2} + \frac{T\alpha^2}{C_p} \tag{1a}$$

and

$$\frac{\delta C_\rho}{\delta\rho} = -T\frac{\delta^2 V}{\delta T^2}. \tag{1b}$$

Here, ρ, c, α, C_p, and V are, respectively, the mass density, speed of sound, volume coefficient of thermal expansion, specific heat, and specific volume. To solve these equations, one requires both speeds of sound across a range of pressures and temperatures, and the densities and specific heats at one (usually low) initial pressure from which integration begins. Solution of these equations proceeds by first integrating Eqn. 1a with the assumption that the term in α and C_p (which corrects from an adiabatic to isothermal path) is negligible. The resulting values of density are used to calculate approximations to

the temperature derivatives of V and, with Eqn. 1b, to C_p. These values are then used in the next integration of Eqn. 1a and the process is reiterated until convergence. The numerical process was validated by reproducing the densities and specific heats of the EOS of Wagner and Pruss (2002), starting from its speeds of sound.

To obtain ρ and C_p at a suitable, initial pressure, it is necessary to interpolate between our results which start at essentially 1 GPa and lower pressures at which ρ and C_p have been measured. Of particular utility in this connection is the EOS of Wagner and Pruss (2002) (adopted in 1995 by the International Association for the Properties of Water and Steam and hereafter designated IAPWS-95). IAPWS-95 is supported by an extensive collection of data at pressures below 1 GPa and, further, was designed to extrapolate reasonably where data were absent. Within the range of our experimental temperatures, uncertainties in densities predicted by IAPWS-95 at 1 GPa are given (Wagner and Pruss, 2002) as 0.1% or better; however, for temperatures above ~60°C uncertainties in specific heats are not given. Comparison with our measured data shows that the specific heats (Fig. 3) predicted by IAPWS-95 are within 2% of our determinations up to ~0.9 GPa and 110°C. The predicted specific heats are also within 3% of the data of Czarnota (1984), except for her two highest points which latter, whether correctly measured or not (see Appendix 1), will be seen to have little consequence for our calculations.

At higher temperatures for which we have not measured specific heats, we can judge the adequacy of IAPWS-95 by comparison with our measured speeds of sound. In Figure 4 fractional deviations between sound speeds predicted by IAPWS-95 and experimentally determined speeds are plotted as a function of pressure for all isotherms. The plotted uncertainties include both those associated with the pressure measurement and with the speed measurement. Uncertainties are larger at low pressure where the pressure derivative of speed is larger. At 1 GPa and now higher temperatures, where measurements of specific heat do not exist, IAPWS-95 sound speeds are in accord with those measured in this study. On this basis, IAPWS-95 is accepted as giving an adequate representation of the thermodynamic properties of water near 1 GPa and up to 400°C, and thus provides suitable starting values for integration of Eqn. 1.

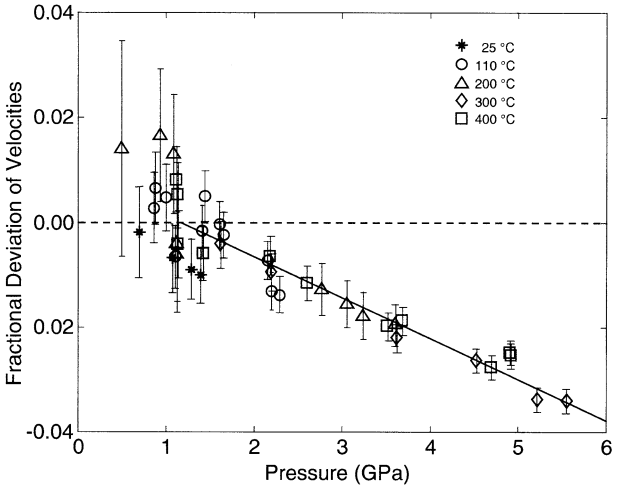

Fig. 4. Fractional deviations of the measured speeds of sound from those predicted by IAPWS-95 (Wagner and Pruss, 2002). Error bars are calculated on the basis of the uncertainties in both speed and pressure; the larger estimated errors near 1 GPa are due to the greater variation of speed with pressure. The continuous line through the data represents a correction which, when applied to the IAPWS-95 velocities, allows calculation of our new equation of state.

Table 2. Calculated densities (g cm^{-3}).

T (°C) / P (GPa)	100	150	200	250	300	350	400
1.0	1.2010	1.1768	1.1526	1.1283	1.1042	1.0802	1.0564
1.2	1.2298	1.2063	1.1830	1.1600	1.1372	1.1146	1.0924
1.4	1.2557	1.2328	1.2104	1.1883	1.1666	1.1452	1.1241
1.6	1.2795	1.2571	1.2354	1.2141	1.1932	1.1727	1.1527
1.8	1.3013	1.2795	1.2584	1.2377	1.2176	1.1979	1.1786
2.0	1.3216	1.3003	1.2797	1.2592	1.2402	1.2211	1.2026
2.2	1.3407	1.3198	1.2997	1.2802	1.2612	1.2428	1.2248
2.4	—	1.3382	1.3185	1.2995	1.2810	1.2630	1.2456
2.6	—	1.3555	1.3363	1.3177	1.2996	1.2821	1.2651
2.8	—	1.3720	1.3532	1.3350	1.3173	1.3002	1.2836
3.0	—	1.3877	1.3693	1.3514	1.3342	1.3174	1.3012
3.2	—	—	1.3847	1.3672	1.3502	1.3339	1.3180
3.4	—	—	1.3994	1.3823	1.3657	1.3496	1.3340
3.6	—	—	1.4137	1.3968	1.3805	1.3647	1.3494
3.8	—	—	1.4274	1.4108	1.3947	1.3792	1.3642
4.0	—	—	—	1.4243	1.4085	1.3933	1.3785
4.2	—	—	—	1.4374	1.4218	1.4068	1.3923
4.4	—	—	—	1.4500	1.4347	1.4200	1.4057
4.6	—	—	—	1.4623	1.4473	1.4327	1.4186
4.8	—	—	—	1.4743	1.4594	1.4451	1.4312
5.0	—	—	—	—	1.4713	1.4571	1.4434
5.2	—	—	—	—	1.4828	1.4688	1.4553
5.4	—	—	—	—	1.4940	1.4802	1.4668
5.6	—	—	—	—	1.5050	1.4914	1.4781
5.8	—	—	—	—	1.5157	1.5022	1.4892
6.0	—	—	—	—	1.5262	1.5128	1.4999

As seen in Figure 4, nearly all deviations of our data from IAPWS-95 lie on a common line within our estimate of uncertainty. Below 1.2 GPa the differences between calculated and measured speeds are within experimental uncertainty, while beyond 1.2 GPa the average deviation increases linearly with increment in pressure, reaching 3% at 5 GPa. To obtain speeds of sound on a dense grid suitable for numerical solution of Eqn. 1, we thus first calculated speeds of sound from IAPWS-95 and subsequently brought these quantities into accord with the experimental results by application of the correction shown as the straight line in Figure 4. Integration of Eqn. 1 was then initiated at 1.0 GPa, with the necessary values of ρ and C_p at that pressure given by IAPWS-95. This process yielded a stable solution and a new EOS.

3.3.2. Equation of state to 6 GPa

Calculated densities are given in Table 2 along several isotherms and are shown in Figure 5a, plotted as deviations from IAPWS-95. Because the measured sound speeds are lower than predicted by IAPWS-95, water is more compressible and densities larger (0.7% at 6 GPa). Specific heats (Fig. 5b) are within 0.5% of those predicted by IAPWS-95, while thermal expansivities are lower by 2% at 6 GPa; however, these two quantities have larger associated uncertainties.

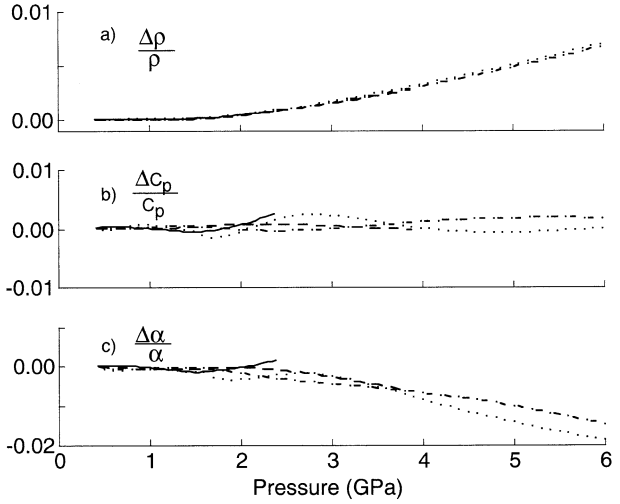

Fig. 5. Calculated densities (a), specific heats (b), and thermal expansivities (c) are shown as fractional deviations from IAPWS-95 (Wagner and Pruss, 2002) along isotherms of 100°C (solid curve), 200°C (dashed), 300°C (dot-dash), and 400°C (dotted). The first two isotherms are plotted only up to their freezing points.

Within the constraints of our data, an acceptable representation of the fractional density deviations in Figure 5a can be given by the third-order polynomial:

$$\Delta\rho/\rho = (\sum_{i=0}^{3} a_i P^i) \times 10^{-4} \qquad (2)$$

with

$$a_0 = 2.0,\ a_1 = -6.8,\ a_2 = 4.75 \text{ and } a_3 = -0.286.$$

Here, P is in units of GPa and the a_i are independent of temperature. Densities for a new, high-pressure EOS are then defined through multiplication of IAPWS-95 densities by the factor $(1 + \Delta\rho/\rho)$. Acceptance of the values of IAPWS-95 at 1 GPa and application of Eqn. 1 completes the new EOS and gives all other thermodynamic quantities.

Speeds of sound calculated from this new EOS are shown as solid lines in Figure 2. Differences between our measured and calculated values are within the estimated experimental errors (Fig. 6).

3.3.3. Estimation of errors

It is important to note that the amount by which the measured speeds of sound differ from IAPWS-95 is significantly larger than any experimental error. Fractional differences of 3% at 5 GPa are 15 times larger than the accuracy with which speed of sound was measured; if attributed to error in pressure measurement, these differences require corrections of 0.55 GPa, which is almost 30 times larger than the experimental precision and would imply an unreasonably large error of 10% in the experimental pressure scale.

In our calculations, variation of the initial densities and specific heats within reasonable estimates of their own uncertainties, variation of the experimental pressure calibration within reasonable estimates of its uncertainty, and use of other starting pressures and interpolation schemes all give substantially the same results. For instance, incrementing the initial (1.0 GPa) densities by 0.1% (the suggested uncertainty in IAPWS-95) shifts all calculated densities by the same amount. Increasing all initial specific heats by 8% (the maximum deviation from IAPWS-95 of Czarnota's two highest pressure points) likewise shifts all calculated C_p by the same amount while decreasing the calculated densities by 0.2% at 6 GPa. A hypothetical, systematic 1% error in the experimental pressure scale also generates a 0.1% change in density at 6 GPa, while a systematic increase in the speeds of sound of 0.1% (the nominal accuracy of our normal calibrant) decreases density by 0.05%.

We consider the possible errors listed above to be the primary source of uncertainty in our EOS and the propagated errors to be a measure of the total uncertainty in calculated density. We therefore conclude that water is 0.7% denser than predictions of IAPWS-95 at 6 GPa, and that at this pressure the absolute uncertainty of the density as given by the new EOS is 0.3%. Thermal expansivities and specific heats are less well constrained as they are more sensitive to higher order derivatives within the calculations, but are within a few percent of those produced by IAPWS-95.

3.4. Comparison With Other Data and Extension to 40 GPa

3.4.1. Shock wave data and equation of state to 40 GPa

For many purposes it would be useful to extend the EOS to pressures and temperatures beyond those reached by these current experiments. Published shock wave data (Walsh and Rice, 1957; Mitchell and Nellis, 1982) have densities along the Hugoniot (the locus of shocked states) that also fall somewhat above those of IAPWS-95 (Fig. 7). Further, up to a pressure of 40 GPa the density deviations exhibit a reasonable continuation of those deduced from our speed of sound data (the thicker line in Fig. 7), even as the shock temperature rises to ~3000 K. (Beyond 40 GPa there is a different variation in the deviations,

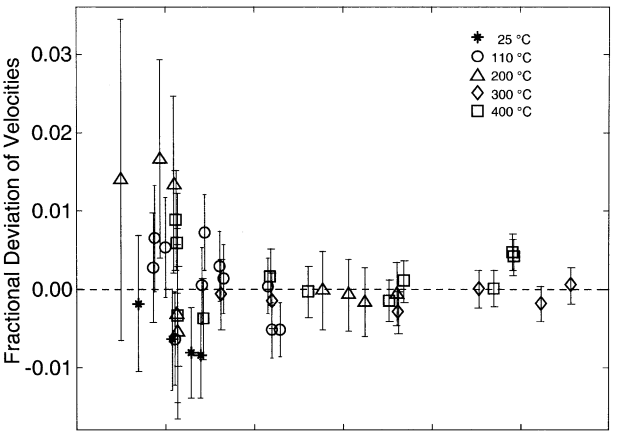

Fig. 6. Fractional deviations of the measured speeds of sound from those predicted by the new equation of state. The residuals are within estimated uncertainties, with the exception of those of the metastable fluid along the 25°C isotherm (*).

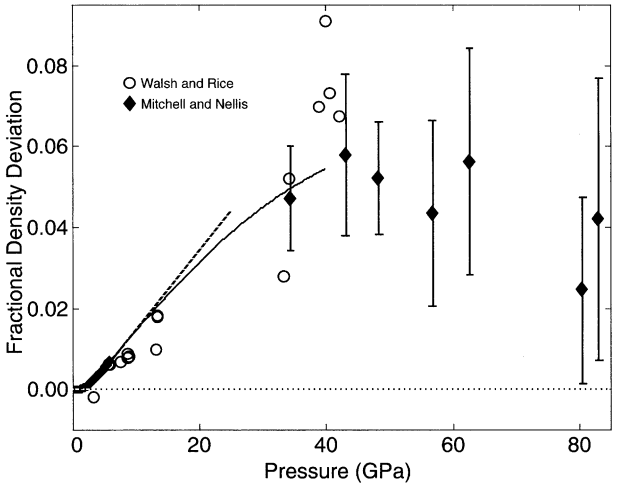

Fig. 7. Fractional deviation of measured densities from those predicted by IAPWS-95 (Wagner and Pruss, 2002) along the shock Hugoniot. The thicker line at lower pressures represents Eqn. 2, derived from our data as shown in Figure 5a; its dashed continuation is in accord with the data of Walsh and Rice (1957) but does not go through the newer, higher pressure data of Mitchell and Nellis (1982). (Associated temperatures can be seen in Fig. 8b.) The continuous line shown up to 40 GPa is a suggested correction on IAPWS-95, defined by Eqns. 2 and 3.

possibly due to a large degree of ionization of the fluid (Mitchell and Nellis, 1982)).

We suggest that up to a pressure of 40 GPa, a temperature of 3000 K, and a density of 2.3 g cm^{-3}, an EOS is best estimated as a temperature-independent density correction to IAPWS-95, given by the curve in Figure 7. For pressures between 1 and 6 GPa, the curve is represented by Eqn. 2 as given above, whereas for pressures between 6 and 40 GPa we have:

$$\Delta\rho/\rho = \left(\sum_{i=0}^{3} b_i P^i\right) \times 10^{-4} \tag{3}$$

with

$$b_0 = -44,\ b_1 = 19.5,\ b_2 = -0.06 \text{ and } b_3 = -0.0015.$$

Other thermodynamic variables can then be determined from this established function in conjunction with the IAPWS-95 values at 1 GPa.

Measured shock densities are shown in Figure 8a as functions of pressure. The thicker line in the figure represents a Hugoniot calculated by application of the Rankine-Hugoniot relations to the new EOS (see Appendix 2). Also shown are calculated shock densities for IAPWS-95, and for the EOS of

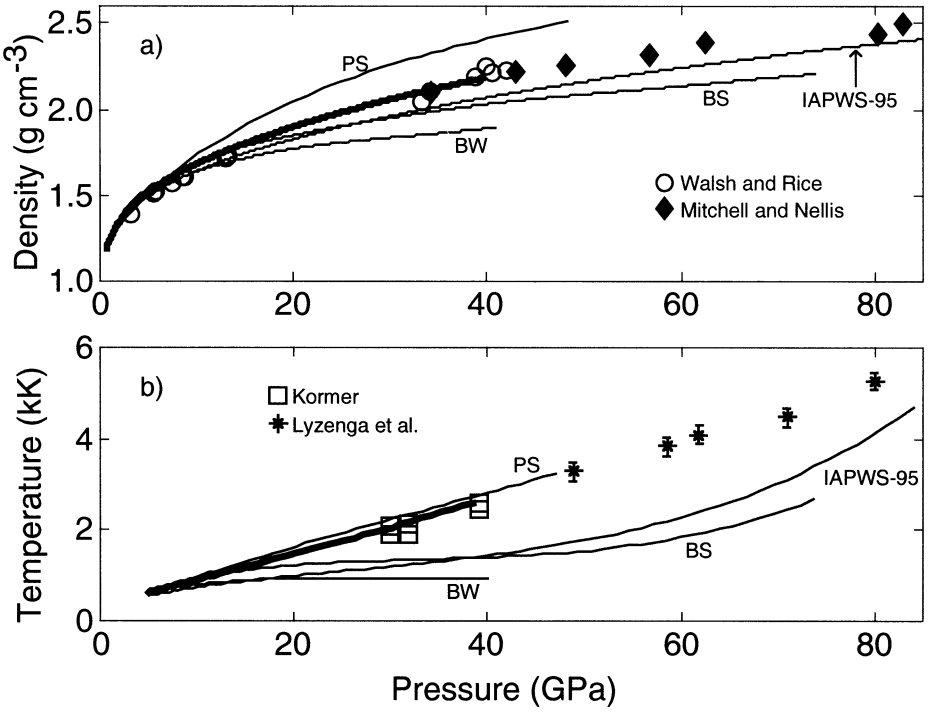

Fig. 8. Absolute densities (a) and temperatures (b) along the Hugoniot are plotted against pressure. Pressures and densities were measured by Walsh and Rice (1957) and by Mitchell and Nellis (1982), while temperatures were measured by Kormer (1968) and Lyzenga et al. (1982). Also shown are curves calculated from various EOS. In (a) the various EOS are allowed to define their own Hugoniot, whereas in (b) the path is forced to fit the measured P-ρ data shown in (a). The thicker lines up to 40 GPa represent the new EOS. IAPWS-95 (Wagner and Pruss, 2002), which was loosely constrained by the shock data, gives densities progressively lower than those measured and, when forced to fit the measured densities, lower temperatures. Calculations based on the EOS of Brodholt and Wood (1993, BW), Belonoshko and Saxena (1991, BS), and Pitzer and Sterner (1994, PS) are also shown. The EOS of Brodholt and Wood (1993) was stated by those authors to be valid only up to a pressure of 30 GPa and temperature of 2000 K; in this figure we show also its extrapolation.

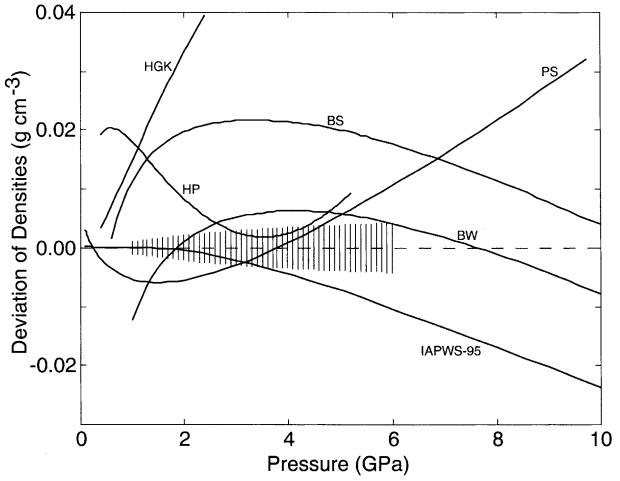

Fig. 9. Absolute density deviations of several other EOS from ours are plotted up to 10 GPa along a 400°C isotherm. HGK, Haar et al. (1984); HP, Holland and Powell (1991); BS, Belonoshko and Saxena (1991); BW, Brodholt and Wood, (1993); PS, Pitzer and Sterner (1994); IAPWS-95, Wagner and Pruss (2002). The shaded area contains the estimated uncertainty for densities calculated from the new EOS; uncertainties beyond 6 GPa are still undetermined.

Belonoshko and Saxena (1991), Brodholt and Wood (1993), and Pitzer and Sterner (1994).

Shock temperatures have been measured directly (Kormer, 1968; Lyzenga et al., 1982) and are displayed in Figure 8b as functions of pressure. Here, we also show the temperatures calculated for each EOS at the pressures and densities measured in the shocks. While our current EOS was modified to better fit the shock-wave pressure-density data shown in Figures 7 and 8a, the concomitant match to measured pressure-temperature points (Fig. 8b) is an independent check on the EOS. IAPWS-95, which gives a reasonable fit to the measured temperatures when allowed to define its own P-ρ path along the Hugoniot, does not do as well in Figure 8b when required to follow the P-ρ relationship given by the experimental data. With the exception of that of Pitzer and Sterner (1994), the other plotted EOS do not adequately fit the temperature data. Only our current EOS fits the shock data in both the comparisons.

Differences in density between our EOS and several of those previously published are shown in Figure 9 along a 400°C isotherm and up to a pressure of 10 GPa. Included in the figure are estimated uncertainties based on the possible errors discussed in section 3.3.3. This provides the first experimentally supported estimate of uncertainties for an EOS of water in this pressure range. With the exception of the EOS of Haar et al. (1984), all those shown are within ~0.04 g/cm^3 of our experimental determination, but still outside the error bounds which have now been established.

3.4.2. *Data from inclusions and expanding capsules*

Several studies have been reported at pressures comparable to those in the present study, but at significantly higher temperatures (700–1600°C). In one such study (Larrieu and Ayers, 1997), the authors used an irreversibly deforming, platinum capsule to record the maximum volumes attained by the included water under known conditions of pressure and temperature. In three other studies (Brodholt and Wood, 1994; Frost and Wood, 1997; Withers et al., 2000) synthetic inclusions in corundum were established at conditions of high pressure and temperature, quenched, and the recovered material analyzed with the presumption that leakage of water trapped in the inclusions was insignificant.

In Figure 10a data from the inclusion studies are plotted against temperature as deviations from our EOS. (The data that derive from an expanding platinum capsule are scattered on this scale and do not offer much guidance.) These three data sets give densities that are lower than those based on our EOS, and the deviations appear to increase systematically with temperature; plotted against pressure or density the same data show no obvious trends. One possible explanation of the discrepancies is that our EOS does not extrapolate well into this region of higher temperatures (and mostly lower densities), and that the resulting error is primarily a function of temperature. Another possibility is that densities deduced from the inclusion studies are systematically in error.

Both in Brodholt and Wood (1994) and in Frost and Wood (1997) the set of inclusions produced by each run is characterized by a maximum, a minimum, and an average observed density. The authors preferred to use averaged densities as the best estimate of the true values, and these are what we have plotted in Figure 10a. However, the scatter recorded within a run is not the result of the measurement process after quenching, but rather indicates a true variation of density among the many recovered inclusions. (Densities are determined by the temperature of phase homogenization, which is measured re-

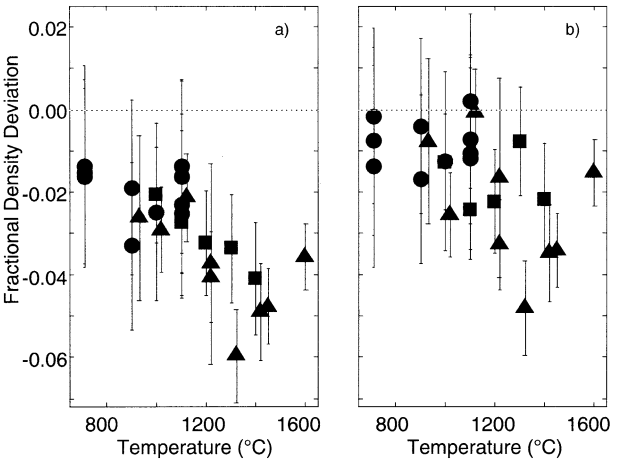

Fig. 10. Fractional differences between densities calculated from inclusion studies and those calculated from our EOS are plotted against temperature. Brodholt and Wood (1994), triangles; Frost and Wood (1997), squares; Withers et al. (2000), circles. In (a) the data are plotted using an average density for each run. In (b) the maximum recorded densities are used. In the case of Withers et al. (2000), the densities inferred from their measurements were based substantially on calibrations against the results of the two other studies and have in (b) been appropriately adjusted to reflect a calibration based on maximum recorded densities. Error bars are calculated on the basis of reported uncertainties in both pressure and temperature for the data of Brodholt and Wood and of Frost and Wood, and on the basis of the uncertainty in chemical shift as given by Withers et al.

producibly to within 1°C for each inclusion, but varies by a far greater amount among inclusions from a single run.) Further, it was shown by Brodholt and Wood (1994) that a slower quench affords both higher average densities and a reduced scatter due, the authors conclude, to lower overall leakage of the inclusions. We therefore hypothesize that all inclusions leak to some extent and that the *highest* measured density in any run defines a lower bound for the true density. A new plot of the inclusion data, using not the averaged but the maximum recorded densities for each run, yields the results shown in Figure 10b. The previously apparent trend with temperature has largely disappeared; perhaps it is due to a higher overall leakage from the inclusions quenched from higher temperatures. Further, it is not difficult to construe the data as defining a lower limit in density which is in accord with our proposed EOS. The possibility that our EOS (essentially that of Wagner and Pruss, 2002, at these lower pressures and this scale of uncertainty) can be extrapolated accurately into this region, and that the inclusion data should be interpreted as a lower bound on density, must then be considered as a reasonable hypothesis.

4. CONCLUSION

We have obtained direct measurements of the speed of sound in water up to 400°C and 5.5 GPa. An experimentally supported EOS is given for these temperatures and pressures, defined by a density correction to IAPWS-95 coupled with acceptance of IAPWS-95 values at 1 GPa; at 6 GPa the associated uncertainty in density is estimated as 0.3%. When extrapolated, the results merge with the higher pressure shock data, leading to the conclusion that this equation of state can be reasonably extended to 40 GPa, 3000 K, and 2.3 g cm^{-3}, across much of the region relevant to our understanding of Earth's mantle.

Acknowledgments—We thank J. P. Brodholt both for his useful criticism of the original manuscript and for his discussion of the inclusion experiments, and also J. M. Zaug for providing us with a sample of the borate pressure calibrant made in his laboratory. This work was supported by Grant No. EAR 01-06683 from the National Science Foundation and by research subcontract #B516166 from Lawrence Livermore National Laboratory.

Associate editor: B. Mysen

REFERENCES

Abramson E. H., Slutsky L. J., and Brown J. M. (1999a) Thermal diffusivity of fluid oxygen to 12 GPa and 300°C. *J. Chem. Phys.* **111,** 9357–9360.

Abramson E. H., Brown J. M., and Slutsky L. J. (1999b) Applications of impulsive stimulated scattering in the earth and planetary sciences. *Annu. Rev. Phys. Chem.* **50,** 279–313.

Abramson E. H., Brown J. M., and Slutsky L. J. (2001) The thermal diffusivity of water at high pressures and temperatures. *J. Chem. Phys.* **115,** 10461–10463.

Belonoshko A. and Saxena S. K. (1991) A molecular dynamics study of the pressure-volume-temperature properties of super-critical fluids: I. H_2O. *Geochim. Cosmochim. Acta* **55,** 381–387.

Bridgman P. W. (1942) Freezing parameters and compressions of twenty-one substances to 50,000 kg/cm^2. *Am. Acad. Arts Sci.* **74,** 399–424.

Brodholt J. and Wood B. (1993) Simulations of the structure and thermodynamic properties of water at high pressures and temperatures. *J. Geophys. Res.* **98,** 519–536.

Brodholt J. P. and Wood B. J. (1994) Measurements of the PVT properties of water to 25 kbars and 1600°C from synthetic fluid inclusions in corundum. *Geochim. Cosmochim. Acta* **58,** 2143–2148.

Czarnota I. (1984) Heat capacity of water at high pressure. *High Temp.-High Press.* **16,** 295–302.

Datchi F., Letoullec R., and Loubeyre P. (1997) Improved calibration of the SrB_4O_7: Sm^{2+} optical pressure gauge: Advantages at very high pressures and high temperatures. *J. Appl. Phys.* **81,** 3333–3339.

Datchi F., Loubeyre P., and LeToullec R. (2000) Extended and accurate determination of the melting curves of argon, helium, ice (H_2O), and hydrogen (H_2). *Phys. Rev. B* **61,** 6535–6546.

Frost D. J. and Wood B. J. (1997) Experimental measurements of the properties of H_2O-CO_2 mixtures at high pressures and temperatures. *Geochim. Cosmochim. Acta* **61,** 3301–3309.

Fujishiro I., Piermarini G. J., Block S., and Munro R. G. (1982) Viscosities and glass transition pressures in the methanol-ethanol-water system. In *High Pressures in Research and Industry: 8th AIRAPT Conference/19th EHPRG Conference, 17–22 August 1981, Institute of Physical Chemistry, University of Uppsala, Sweden: Proceedings* (eds. C.-M. Backman, T. Johannisson, and L. Tegner), pp. 608–611. Arkitektkopia, Uppsala.

Haar L., Gallagher J. S., and Kell G. S. (1984) NBS/NRC Steam Tables: Thermodynamic and transport properties and computer programs for vapor and liquid states of water in SI units. Hemisphere Publishing, Washington, D.C.

Holland T. and Powell R. (1991) A compensated-Redlich-Kwong (CORK) equation for volumes and fugacities of CO_2 and H_2O in the range 1 bar to 50 kbar and 100–1600°C. *Contrib. Mineral. Petrol.* **109,** 265–273.

Kormer S. B. (1968) Optical study of the characteristics of shock-compressed condensed dielectrics. *Sov. Phys. Uspekhi.* **11,** 229–254 (figure on p. 239).

Larrieu T. L. and Ayers J. C. (1997) Measurements of the pressure-volume-temperature properties of fluids to 20 kbar and 1000°C: A new approach demonstrated on H_2O. *Geochim. Cosmochim. Acta* **61,** 3121–3134.

Lawson A. W., Lowell R., and Jain A. L. (1959) Thermal conductivity of water at high pressures. *J. Chem. Phys.* **30,** 643–647.

Lyzenga G. A., Ahrens T. J., Nellis W. J., and Mitchell A. C. (1982) The temperature of shock-compressed water. *J. Chem. Phys.* **76,** 6282–6286.

Mao H. K., Xu J., and Bell P. M. (1986) Calibration of the ruby pressure gauge to 800 kbar under quasi-hydrostatic conditions. *J. Geophys. Res.* **91,** 4673–4676.

Mitchell A. C. and Nellis W. J. (1982) Equation of state and electrical conductivity of water and ammonia shocked to the 100 GPa (1 Mbar) pressure range. *J. Chem. Phys.* **76,** 6273–6281.

Pei Z., Su Q., and Zhang J. (1993) The valence change from RE^{3+} to RE^{2+} (RE≡Eu, Sm, Yb) in SrB_4O_7: RE prepared in air and the spectral properties of RE^{2+}. *J. Alloys Comp.* **198,** 51–53.

Pitzer K. S. and Sterner S. M. (1994) Equations of state valid continuously from zero to extreme pressures for H_2O and CO_2. *J. Chem. Phys.* **101,** 3111–3116.

Saul A. and Wagner W. (1989) A fundamental equation for water covering the range from the melting line to 1273 K at pressures up to 25000 MPa. *J. Phys. Chem. Ref. Data* **18,** 1537–1564.

Wagner W., Saul A., and Pruss A. (1994) International equations for the pressure along the melting and along the sublimation curve of ordinary water substance. *J. Phys. Chem. Ref. Data* **23,** 515–525.

Wagner W. and Pruss A. (2002) The IAPWS Formulation (1995) for the thermodynamic properties of ordinary water substance for general and scientific use. *J. Phys. Chem. Ref. Data* **31,** 387–535.

Walsh J. M. and Rice M. H. (1957) Dynamic compression of liquids from measurements on strong shock waves. *J. Chem. Phys.* **26,** 815–830.

Wiryana S., Slutsky L. J., and Brown J. M. (1998) The equation of state of water to 200°C and 3.5 GPa: Model potentials and the experimental pressure scale. *Earth Planet. Sci. Lett.* **163,** 123–130.

Withers A. C., Kohn S. C., Brooker R. A., and Wood B. J. (2000) A new method for determining the P-V-T properties of high-density H_2O using NMR: Results at 1.4–4.0 GPa and 700–1100°C. *Geochim. Cosmochim. Acta* **64,** 1051–1057.

APPENDIX 1

Specific Heat of Water Near the Fluid-Ice VI Phase Boundary

A side issue which presents itself is whether the measurements of specific heat taken by Czarnota (1984) are accurate at the two highest pressures recorded (see Fig. 3); i.e., does the specific heat of cool water increase rapidly with pressure near the fluid–ice VI phase boundary at ~1 GPa? Because the conductivity data of Lawson et al. (1959) terminate at a pressure of 0.8 GPa, it is not possible for us to make a direct comparison through our measurements of diffusivity; however, we may consider two different possibilities.

The pressures and temperatures at which these points were taken are within the uncertainty limits of the fluid–ice VI phase boundary (Wagner et al., 1994); it would not be unreasonable to suppose that somewhere in the apparatus small amounts of ice had formed. This would presumably lead to larger measured values of heat capacity and be interpreted as indicating a larger specific heat.

On the other hand, it is interesting to note that measured diffusivities at 25°C have a qualitatively different behavior than do those at higher (>100°C) temperatures (Abramson et al., 2001). Moreover, two measurements of diffusivity made at 25°C, but in the metastable fluid at 1.08 and 1.27 GPa, indicate an abrupt departure from the trend of the lower pressure data (Abramson et al., 2001), and Figure 4 shows a small, but apparently significant, systematic difference between the behavior of speeds of sound measured at 25°C and others measured at higher temperatures.

We cannot, therefore, rule out the possibility that, below ~100°C and in or near the metastable regime, the actual values of C_p increase rapidly with pressure in a manner not reproduced by IAPWS-95, nor by our EOS. These observations are pertinent to the study of the anomalous properties of cool water, but are likely of little consequence to an EOS of the hot fluid. As reported above, variation of the initial values of C_p, even within the uncertainty suggested by the two points under consideration, has little effect on the resulting calculated densities, which are strictly constrained by the measured speeds of sound.

APPENDIX 2

Calculation of Shock Pressures and Densities

The final state attained after passage of a shock wave is given by the Rankine-Hugoniot relations, derived from the conservation of momentum, mass, and energy:

$$P_1 - P_0 = U_s U_p / V_0 \tag{A1}$$

$$V_1/V_0 = (U_s - U_p)/U_s \tag{A2}$$

$$E_1 - E_0 = (P_1 - P_0)(V_0 + V_1)/2 \tag{A3}$$

where P, V, and E denote the pressure, specific volume, and specific internal energy, the subscripts 0 and 1 denote values before and after passage of the shock, respectively, U_s represents the shock speed, and U_p the speed to which the material has been accelerated behind the shock. In a typical set of experiments U_s and U_p are measured for each of several different impressed shock speeds, allowing calculation of the final state parameters for each of these shocks. If a full EOS is known, or assumed, the variables P, V, and E can be readily converted into the more useful variables P, V, and T. Final temperatures can also be measured independently.

For Figure 8a, theoretical Hugoniot curves were determined by calculating shock pressures and temperatures for each of a set of shock densities. For each density, a temperature was sought such that P_1 and E_1, as given by the EOS, also satisfied Eqn. A3. In the case of the EOS of Belonoshko and Saxena (1991), which describes only the relations among pressure, volume, and temperature, we assumed that at the lowest pressure (0.5 GPa) for which this EOS is defined the internal energies are adequately given by IAPWS-95 (which assumption is sufficient to calculate all energies at higher pressures). For the EOS of Brodholt and Wood (1993) we have used their calculated internal energies, tabulated in that paper.